Ionic Wave Propagation along Actin Filaments

J. A. Tuszyński,* S. Portet,* J. M. Dixon,* C. Luxford,* and H. F. Cantiello†
*Department of Physics, University of Alberta, Edmonton, Alberta T6G 2J1, Canada; and †Massachusetts General Hospital and Harvard Medical School, Charlestown, Massachusetts 02129 USA

ABSTRACT We investigate the conditions enabling actin filaments to act as electrical transmission lines for ion flows along their lengths. We propose a model in which each actin monomer is an electric element with a capacitive, inductive, and resistive property due to the molecular structure of the actin filament and viscosity of the solution. Based on Kirchhoff's laws taken in the continuum limit, a nonlinear partial differential equation is derived for the propagation of ionic waves. We solve this equation in two different regimes. In the first, the maximum propagation velocity wave is found in terms of Jacobi elliptic functions. In the general case, we analyze the equation in terms of Fisher-Kolmogoroff modes with both localized and extended wave characteristics. We propose a new signaling mechanism in the cell, especially in neurons.

INTRODUCTION

The cytoskeleton is a major component of all living cells. It is made up of three different types of filamental structures, including actin-based microfilaments (MFs), intermediate filaments (e.g., neurofilaments, keratin), and tubulin-based microtubules (MTs). All of them are organized into networks, which are interconnected through numerous particular proteins, and which have specific roles to play in the functioning of the cell. The cytoskeletal networks are mainly involved in the organization of different directed movements in cell migration, cell division, or in the internal transport of materials. Polymerization of MFs is responsible for cell migration and for the remodeling of the leading edge of cells. MTs attach to the chromosomes and mediate cell division. Molecular motors are protein complexes that are associated with the cytoskeleton and drive organelles along MTs and MFs in a ''vectorial'' transport.

Actin is the most abundant protein in the cytoplasm of mammalian cells, accounting for 10–20% of the total cytoplasmic protein content. Actin exists either as a globular monomer (Fig. 1), i.e., as the so-called G-actin, or as a filament, i.e., an MF: the globular monomers polymerize into polar two-stranded helical polymers, MFs, also called F-actin. Under physiological conditions, actin filaments are one-dimensional polymers that behave as highly charged polyelectrolytes (Cantiello et al., 1991; Kobayasi, 1964; Kobayasi et al., 1964). The linear charge density of F-actin is estimated theoretically to be 4×10^3 e/μm in vacuum, and although lower than that of DNA at physiological pH, it may support ionic condensation in buffer solutions as originally predicted by Manning's condensation theory (Manning, 1978). This has recently been confirmed experimentally by light scattering (Tang and Janmey, 1996) although other experimental work arrives at linear charge densities that are much higher (Cantiello et al., 1991) of order 1.65×10^5 e/μm. The latter value of charge density is consistent with other experiments and is associated with a highly uncompensated charge density of actin in solution. These experiments include the coexistence of different electric (Kobayasi, 1964; Kobayasi et al., 1964) and magnetic (Torbet and Dickens, 1984) dipole moments in F-actin, the anomalous Donnan potential, nonlinear electro-osmotic behavior of actin filaments in solution (Cantiello et al., 1991), and the ability of F-actin to support ionic condensation-based waves (Lin and Cantiello, 1993).

Many years ago, Manning (1978) postulated an elegant theory, which stated that polyelectrolytes may have condensed ions in their surroundings. According to Manning's hypothesis, counterions ''condense'' along the stretch of polymer, if a sufficiently high linear charge density is present on the polymer's surface. Thus, a linear polymer may be surrounded by counterions from the saline solution such that counterions are more closely surrounding the polymer's surface, and co-ions of the salt solution are repelled such that a depletion area is also created. Some important details of the ion distribution in polyelectrolytes regarding Manning's condensation theory can be found in Le Bret and Zimm (1984). The sum of surface charges and associated counterions drops to values given by a formula that depends on the valence of the counterions and the Bjerrum length. This parameter, in turn, is a phenomenological property of the ion's ability to compensate for the surface charges, depending on the solvent and temperature of the solution. Bjerrum developed a modification of the Debye-Hückel theory in 1926 for ion-pair formation provided that the ions are small, they are of high valence, and the dielectric constant of the solvent is small (see MacInnes, 1961, for a comprehensive explanation of derivations of relevant equations). The Bjerrum length is the distance at which the Coulomb energy of the screened charges equals k_BT, the thermal energy, creating an equilibrium under which the charges would not preferentially move from that equilibrium. See Eq. 1 below.

Submitted July 16, 2003, and accepted for publication November 14, 2003.
Address reprint requests to J. A. Tuszyński, E-mail: jtus@phys.ualberta.ca.
J. M. Dixon's permanent address is Dept. of Physics, University of Warwick, Coventry CV4 7AL, UK.

0006-3495/04/04/1890/14 $2.00

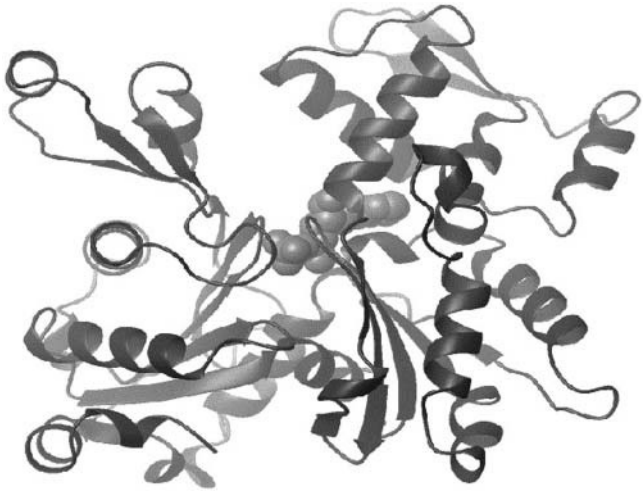

FIGURE 1 Ribbon diagram of an actin monomer (Kabsch et al., 1990) (Protein Data Bank identification: 1ATN). Figure produced with RasMol.

The cylindrical volume of depleted ions outside the cloud of ions surrounding the polymer serves as an electrical shield. Thus, the ''cable-like'' behavior of such a structure is supported by the polymer itself and the ''adsorbed'' counterions, which for all practical purposes are ''bound'' to the polymer. The strength of this interaction is such that even under infinite dilution conditions (i.e., ionic strength $\gtrsim 0$), the counterions are still attracted to the polymer and do not diffuse out from the polymer's vicinity. Although this theory was originally postulated for such polyelectrolytes as DNA, the same applies to highly charged one-dimensional polymers.

Available atomic models of actin are largely derived from the crystal structure of the monomer and primary sequencing (Holmes et al., 1990; Kabsch et al., 1990) and not from actin's behavior in solution. Thus there is the possibility of other explanations to reconcile the discrepancy between theoretical and experimentally determined charge densities of actin. This could include highly nonlinear interactions between the hydrated molecule and its surrounding counterions, which are not taken into account in the atomic models above and which may play an important role in the electrodynamic properties of proteins in solution (Rullman and van Duijnem, 1990). It is to be expected, for example, that, because of the helical nature of the F-actin (Holmes et al., 1990), the distribution of counterions will be nonuniform along the polymer's length. As a consequence, spatially dependent electric fields could be present and arranged in peaks and troughs as originally postulated by Oosawa (1971). This might imply large changes in the density of small ions around the polymer with a large dielectric discontinuity in the ionic distribution (Kabsch et al., 1990; Anderson and Record, 1990).

The double helical structure of the filament provides regions of uneven charge distribution such that pockets of higher and lower charge density may be expected. The charge distribution can be envisioned as a string of cola bottles inside an elastic tube. As the bottles are pushed into the cylinder, the outer shape of the wider parts of each bottle may provide the shortest distance to the cylinder's wall, and thus the thinnest charge density. The thinner sections of each bottle provide ''deeper'' pockets where more ions can be trapped. The distance between ion clusters in the pockets, which in reality are immersed in water with very specific properties not shared by the bulk solution, will make ions move up and down the slopes of the surface of the bottle. This uneven ionic distribution along a short stretch of the polymer (likely the average pitch 35–40 nm) may be considered a linear unit of the circuit to be modeled. This ionic distribution makes two essential contributions to the nonlinear electrical components of the model. First, the nonlinear capacitor, which is associated with the spatial difference in charges between the ions located in the outer and inner regions of the polymer. Second, any charge movement tending to dissipate this local gradient (reversibly) generates a secondary electromotive force due to the charge movement, namely a local current. This is the main contribution to the inductance of the single stretch of polymer.

F-actin, being a highly charged polyelectrolyte, contains a fraction of its surrounding counterions in the form of a condensed cloud about its surface. Such a cloud may be highly insensitive to large changes in the ionic strength of the surrounding saline solution (Oosawa, 1970; Manning, 1969; Zimm, 1986).

The Bjerrum length, λ_B, describes the distance beyond which thermal fluctuations are stronger than the electrostatic attractions or repulsions between charges in solution whose dielectric constant is ε. It is defined by

$$\frac{e^2}{4\pi\varepsilon\varepsilon_0\lambda_B} = k_B T \tag{1}$$

for a given temperature T in Kelvin. Here e is the electronic charge, ε_0 the permittivity of the vacuum, and k_B is Boltzmann's constant. For a temperature of 293 K, it is readily found that $\lambda_B = 7.13 \times 10^{-10}$ m. Counterion condensation occurs when the mean distance between charges, b, is such that $\lambda_B/b = S > 1$. Each actin monomer carries an excess of 14 negative charges in vacuum, and accounting for events such as protonation of histidines, and assuming there to be 3 histidines per actin monomer, there exist 11 fundamental charges per actin subunit (Tang and Janmey, 1996). Assuming an average of 370 monomers per μm, we find that there is ~ 4 e/nm in agreement with an earlier statement. Thus we expect a linear charge spacing of $b = 2.5 \times 10^{-10}$ m, so $S = 2.85$. As the effective charge, q_{eff}, or renormalized rod charge is the bare value divided by S, we find $q_{eff} = 3.93$ e/monomer.

Assuming for simplicity a linear charge distribution about the actin filament, the linear charge density, ξ, is much

greater than $1/z$, where z is the valence of the counterions in solution. The parameter, ξ, is given by

$$\xi = \frac{e^2}{4\pi\varepsilon_0\varepsilon_r k_B T b}, \quad (2)$$

where e is the electronic charge, ε_r the dielectric constant of water, and b the average axial spacing of charges on the polyelectrolyte (Zimm, 1986). The parameter, ξ, was calculated to be 110 for actin filaments (with $z = 1$ for H^+ and K^+ ions) and so $\xi \gg 1/z$ (Lin and Cantiello, 1993). Thus ~99% of the counterion population is predominantly constrained within a radius of 8 nm (Pollard and Cooper, 1986) round the polymer's radial axis (Zimm, 1986). Significant ionic movements within this ''tightly bound'' ionic cloud are therefore allowed along the length of the actin (Fig. 2), provided that it is shielded from the bulk solution (Oosawa, 1970; Parodi et al., 1985).

The electro-conductive medium is a condensed cloud of ions surrounding the polymer. To be electrically insulated from the bulk of the solution (although not mandatory), there should be some sort of shielding from the bulk solution, which acts as a common ground to the ''transmission line''. The presence of one or more layers of waters of hydration around the protein filament may provide additional screening. In earlier publications (Hameroff et al., 2002; Hagan et al., 2002), some of the present authors have suggested that such a condensation/ionic cloud/plasma phase around microtubules may help shield not only signaling but quantum states from external decoherence. In this connection, the transfer of information by quantum coherence-based phenomena requires that the system be isolated from the environment such that the ''energy'' does not dissipate. This would imply that efficient transfer of energy from ''energized groups'' that can only be in resonating frequencies when they are close to each other (Davydov, 1982; Fröhlich, 1975, 1984). In the context of microtubular ''kink'' soliton behavior, the calcium ions adsorbed to one region of each tubulin monomer may form a functional dipole, which is shifted in space by energizing the monomer by GTP binding (Sataric et al., 1993). The dipolar moments of each heterodimer (α-, β-tubulins) would be switched in the microtubule, such that a change in structural local stability is transferred spatially along the microtubular structure. This is the basis of the proposed information transfer mechanism, which although highly probable, is different from the ionic waves supported by actin filaments. It is important to note, however, that ionic waves might also be supported by microtubules, a phenomenon that will require experimental proof. Furthermore, quantum models supported by microtubular structures might also exist that imply a particular state of water in the microtubular structure that indeed has properties largely different from those expected by free solution (see Mavromatos, 1999).

Bearing in mind the sheath of counterions around the actin filament, we see that effectively actin polymers may act as biological ''electrical wires'', which can be modeled as nonlinear inhomogeneous transmission lines that are able to propagate nonlinear dispersive solitary waves (Kolosick et al., 1974; Ostrovskii, 1977) in the form of solitons (Lonngren, 1978; Noguchi, 1974). It has been proposed that such solitons, localized traveling waves, exist in many biological systems and, in fact, have earlier been postulated in linear biopolymers such as MTs (Sataric et al., 1993) and DNA (Baverstock and Cundall, 1988). Interestingly, both solitary waves (Lin and Cantiello, 1993) and liquid crystal formation (Coppin and Leavis, 1992; Furukawa et al., 1993) have been observed in actin filaments possibly providing a potentially fruitful environment for innovative biotechnological applications.

In this article we develop a model based on the transmission line analogy with inductive, resistive, and capacitive components. The physical significance of each of the components, for each section of the electrical network, will be described below. This way we will investigate the nature of nonlinear ionic waves propagating along an actin filament in solutions containing counterions as would be found under realistic physiological conditions.

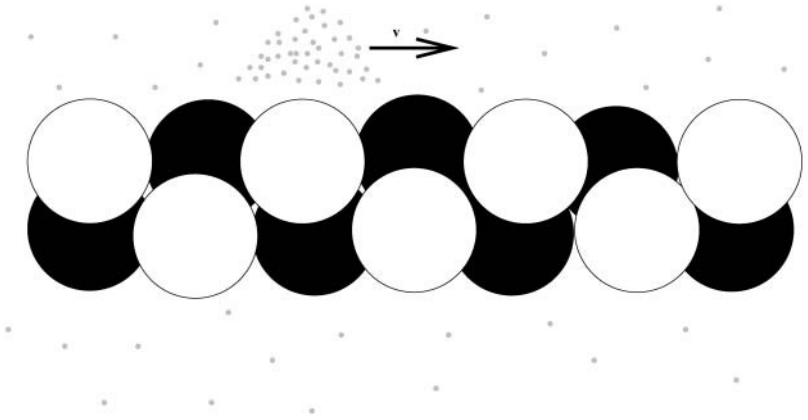

FIGURE 2 Nonlinear dispersive solitary waves traveling along an actin filament.

CHARACTERIZATION OF THE TRANSMISSION LINE COMPONENTS

In this section, we describe the electrical components that make up our nonlinear circuit, which mimics the behavior of an actin filament in solution. As the filament core is separated from the rest of the ions in the bulk solution by the counterion condensation cloud, we expect this cloud to act as a dielectric medium between the two. This cloud provides both resistive and capacitive components for the behavior of the monomers that make up the actin filament. Ion flow is expected at a radial distance from the center of the filament, which is approximately equal to the Bjerrum length. The inductive component to the electrical properties of ionic waves is due to actin's double-stranded helical structure that induces the ionic flow in a solenoidal manner. Below we discuss the origin of each electrical component in turn.

The effective Bjerrum length of an actin filament in solution was derived in Lin and Cantiello (1993) with data originally obtained in Cantiello et al. (1991). In that study, a Donnan potential of ~ -3.93 mV was found for actin in solution.

The origin of capacitance

We first envisage the protein surface negative charge to be distributed homogeneously on a cylinder defining the filament surface. Furthermore, positive counterionic charges in the bulk are expected to form another cylinder at a radius greater than the actin filament itself, $\sim$1 Bjerrum length, λ_B, away from the actin surface, which includes the condensed ions (Fig. 3). The permittivity, ε, is given by $\varepsilon = \varepsilon_0\varepsilon_r$, where ε_r is the relative permittivity, which we take to be that of water, i.e., $\varepsilon_r = 80$. We take the length of an actin monomer typically as $a \simeq 5.4$ nm and the radius of the actin filament, r_{actin}, to be $r_{actin} \simeq 2.5$ nm (Chasan et al., 2002). The next step is to consider a cylindrical Gaussian surface of length a whose radius is r such that

$$r_{actin} < r < r_{actin} + \lambda_B. \tag{3}$$

If the total charge enclosed is Q_{encl}, then from Gauss' law we have

$$\mathbf{E} = \frac{Q_{encl}}{2\pi\varepsilon l}\left(\frac{1}{r}\right)\mathbf{r}. \tag{4}$$

The potential difference between the cylinder representing the filament's surface and the outer cylinder is therefore given by

$$\Delta V = -\int_{r_{actin}}^{r_{actin}+\lambda_B} \mathbf{E}.d\mathbf{r} = -\frac{Q_{encl}}{2\pi\varepsilon l}\ln\left(\frac{r_{actin}+\lambda_B}{r_{actin}}\right), \tag{5}$$

where $d\mathbf{r}$ is an infinitesimal vector in the direction of the radial unit vector $\mathbf{r}$. The capacitance, C_0, is defined by

$$C_0 = \frac{Q_{encl}}{|\Delta V|} \tag{6}$$

so that

$$C_0 = \frac{2\pi\varepsilon l}{\ln\left(\frac{r_{actin}+\lambda_B}{r_{actin}}\right)}. \tag{7}$$

With the parameters given above, we estimate that the capacitance per monomer is $C_0 \simeq 96 \times 10^{-6}$pF.

Evaluating an effective inductance

For actin in solution, a key feature is that the positively charged end assembles more quickly than the negatively charged end (Sept et al., 1999). This results in an asymmetry in the charges at the ends of the filaments and F-actin's electric polarization. Actin monomers arrange themselves head to head to form actin dimers resulting in a probable alternating distribution of electric dipole moments along the length of the filament (Kobayasi, 1964; Kobayasi et al., 1964). We assume, therefore, that there is a helical distribution of ions winding around the filament at approximately a radial distance equal to one Bjerrum length. This may be thought of as a solenoid in which a fluctuating current is flowing as a result of voltage differences generated at each end. This solenoidal flow geometry leads to an equivalent electrical element possessing self inductance (Fig. 4). The

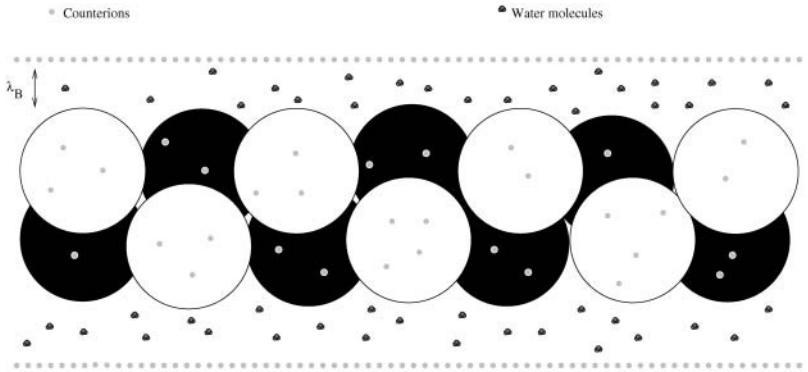

FIGURE 3 Positive counterionic charges in the bulk form a cylinder around the F-actin filament. The distance between this cylinder and the F-actin filament is $\sim$1 Bjerrum length. There also are some counterions that condense to the actin filament.

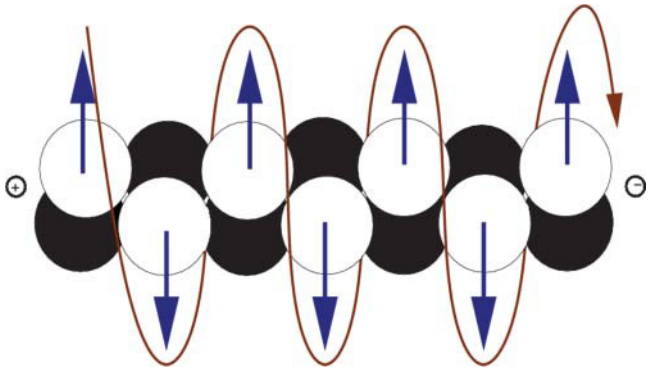

FIGURE 4 Dipole moment of a dimer is represented by the arrow.

magnetic induction field, **B**, inside such a solenoid, parallel to its axis is given by

$$\mathbf{B} = \mu \frac{N}{l} I\mathbf{z}, \tag{8}$$

where **z** is a unit vector along the axis of the solenoid, N is the total number of effective turns of the coil (the number of windings of the helical distribution of ions around the filament), μ is the magnetic permeability, and I the current through the coil. From Faraday's law the *emf* generated is

$$emf = -\left(\frac{\mu N^2 A}{l}\right)\frac{dI}{dt}, \tag{9}$$

where A is the cross-sectional area of the effective coil given by

$$A = \pi(r_{\text{actin}} + \lambda_{\text{B}})^2. \tag{10}$$

The potential drop across an inductance, L, is given by

$$emf = -\left(L\frac{dI}{dt}\right), \tag{11}$$

so we may define an effective inductance for the actin filament in solution by

$$L = \frac{\mu N^2 A}{l}, \tag{12}$$

where l is the length of the F-actin. The number of turns, $N = a/r_{\text{h}}$, is approximated by simply working out how many ions could be lined up along the length of a monomer. We would then be approximating the helical turns as circular rings lined up along the axis of the F-actin. This is surely an overestimate to the number of helical turns per monomer, but it is certainly within reason for our purposes as an initial approximation. We also take the hydration shell of the ions into account in our calculation. This shell results when an ion is inserted into a water configuration, changing the structure of the hydrogen bond network. A water molecule will reorient such that its polarized charge concentration faces the opposite charge of the ion. As the water molecules orient themselves toward the ion, they break the hydrogen bonds to their nearest neighbors. The hydration shell is then the group of water molecules oriented around an ion. A rough estimate for the size of a typical ion in our physiological solution, with a hydration shell, is $r_{\text{h}} \simeq 3.6 \times 10^{-10}$m. This is the approximate radius of the first hydration shell of sodium ions. Substituting these values into Eq. 12, we readily find that $L \simeq 1.7$ pH for the length of the monomer.

Modeling the resistance component

The current, I, between the two concentric cylinders is

$$I = \int \mathbf{J}.d\mathbf{a} = \sigma \int \mathbf{E}.d\mathbf{a} = \frac{\sigma}{\varepsilon}\lambda l, \tag{13}$$

where we have related linearly the current density, **J**, to the electric field by $\mathbf{J} = \sigma\mathbf{E}$, σ being the conductivity and the integral is over an infinitesimal area, $d\mathbf{a}$, on the surface of the outer cylinder pointing radially outward. Using Ohm's law, including the potential difference in Eq. 5 and the current I in Eq. 13, the magnitude of the resistance, $R = V/I$, is given by

$$R = \frac{\rho \ln((r_{\text{actin}} + \lambda_{\text{B}})/r_{\text{actin}})}{2\pi l}, \tag{14}$$

where ρ is the resistivity. To a first-order approximation, the conductivity of a solution as a function of salt concentration, c, obeys the relationship

$$\sigma(c) \simeq \wedge_0 c, \tag{15}$$

where $\wedge_0$ is a positive constant that does not depend on concentration but only on the type of salt. Typically, for K^+ and Na^+, intracellular ionic concentrations are 0.15 M and 0.02 M, respectively (Tuszynski and Dixon, 2001). The $\wedge_0$ parameters for the two ions are

$$\begin{aligned} \wedge_0^{\text{K}^+} &\simeq 7.4(\Omega\text{m})^{-1}\text{M}^{-1} \\ \wedge_0^{\text{Na}^+} &\simeq 5.0(\Omega\text{m})^{-1}\text{M}^{-1}. \end{aligned} \tag{16}$$

Kohlrausch's law states that the molar conductance of a salt solution is the sum of the conductivities of the ions comprising the salt solution. Thus

$$\sigma \simeq \wedge_0^{\text{K}^+} c_{\text{K}^+} + \wedge_0^{\text{Na}^+} c_{\text{Na}^+} = 1.21(\Omega\text{m})^{-1}. \tag{17}$$

Using Eq. 17 with $\rho = \sigma^{-1}$, the resistance estimate in Eq. 14 becomes $R = 6.11$ MΩ, which is very much less, as we would expect, than pure water since $R_{\text{water}} = 1.8 \times 10^6$ MΩ, the physiological solution being much more conductive than pure water.

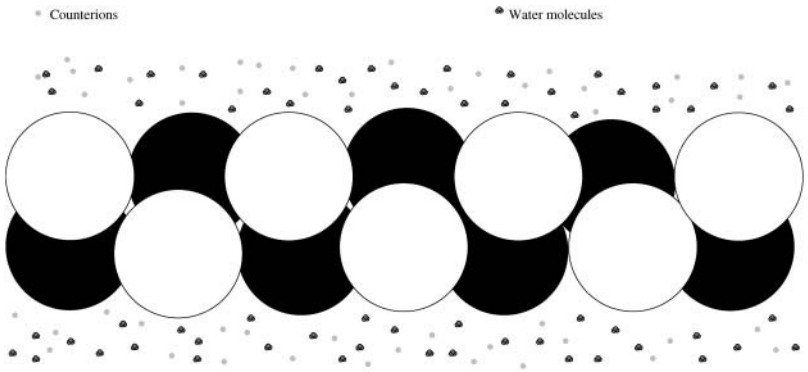

FIGURE 5 F-actin surrounded by water molecules and counterions.

Effective values for F-actin

In the analysis of F-actin surrounded by saline solution (see Fig. 5), it is useful to have values for resistance, inductance, and capacitance for the entire filament. This amounts to finding effective values using the appropriate addition rules. Referring to Fig. 6, we see that we must include both the parallel and series contributions to the resistance, that the total capacitance is a parallel-addition formula, and the total inductance is obviously a strictly series contribution. For a filament containing n monomers, we would get an effective resistance, inductance, and capacitance, respectively, such that:

$$R_{\text{eff}} = \left(\sum_{\text{i}=1}^{\text{n}} \frac{1}{R_{2,\text{i}}}\right)^{-1} + \sum_{\text{i}=1}^{\text{n}} R_{1,\text{i}} \tag{18}$$

$$L_{\text{eff}} = \sum_{\text{i}=1}^{\text{n}} L_{\text{i}} \tag{19}$$

and

$$C_{\text{eff}} = \sum_{\text{i}=1}^{\text{n}} C_{0,\text{i}}, \tag{20}$$

where $R_{1,\text{i}} = 6.11 \times 10^6\ \Omega$ and $R_{2,\text{i}} = 0.9 \times 10^6\ \Omega$ such that $R_{1,\text{i}} = 7R_{2,\text{i}}$. The reader should note that we have used $R_{1,\text{i}} = R_1$, $R_{2,\text{i}} = R_2$, $L_{\text{i}} = L$, and $C_{0,\text{i}} = C_0$.

For a 1 μm of the actin filament, we find therefore

$$R_{\text{eff}} = 1.2 \times 10^9 \Omega$$
$$L_{\text{eff}} = 340 \times 10^{-12}\text{H}$$
$$C_{\text{eff}} = 0.02 \times 10^{-12}\text{F}.$$

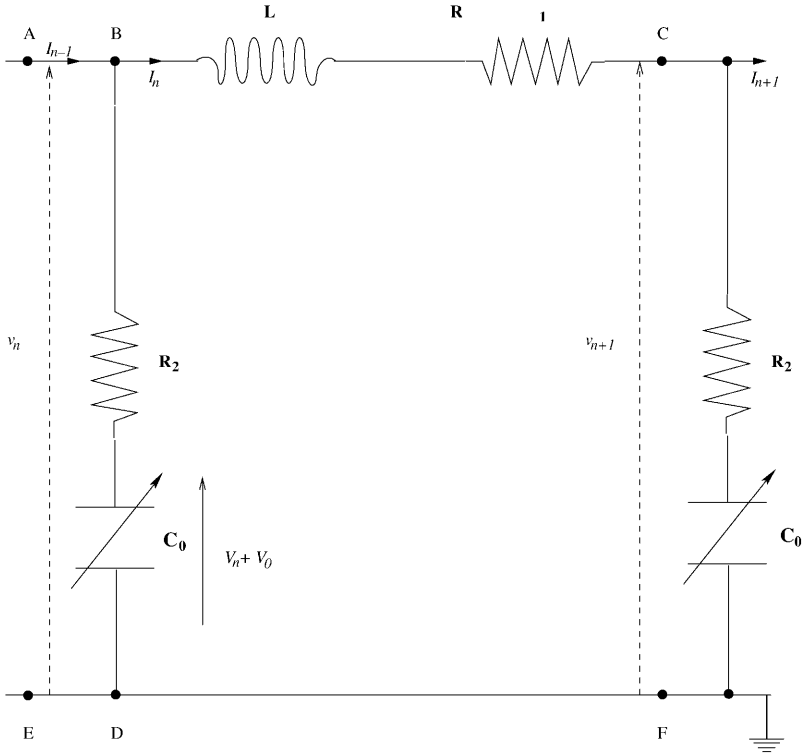

FIGURE 6 An effective circuit diagram for the nth monomer between the dotted lines. I_{n} is the current through the inductance L and resistance R_1.

MODELING ACTIN FILAMENTS AS NONLINEAR LRC TRANSMISSION LINES

In this section, we set up an electrical model of the actin filament, using inductive, capacitive, and resistive components, based on the ideas developed in the last section. Basically, we apply Kirchhoff's laws to that section of the effective electrical circuit for one monomer, M, which involves coupling to neighboring monomers (see Fig. 6). We then take the continuum limit, assuming a large number of monomers along an actin filament.

We expect a potential difference between one end of the monomer generated between the filament core and the ions lying along the filament at one Bjerrum length away. We have already seen that these ''Bjerrum ions'' generate a time-dependent current by movement along helical paths and hence are responsible for the inductance, L. Due to viscosity, we also anticipate a resistive component to these currents, which we insert in series with L and denote it by R_1 (see Fig. 6). In parallel to these components, there exists a resistance, which we call R_2, acting between the Bjerrum ions and the surface of the filament. In series with this resistance, we have a capacitance, C_0. We assume that the charge on this capacitor varies in a nonlinear way with voltage much like the charge-voltage relation for a reversed-biased *pn* diode junction (Ma et al., 1999; Wang et al., 1999). Thus we suppose, for the nth monomer,

$$Q_n = C_0(V_n - bV_n^2), \tag{21}$$

where b is expected to be small.

From Kirchhoff's laws, using Fig. 6, if I_n is the current through the inductance, L, and the resistor R_1 and I_{n-1}, is that flowing along AB, the current in DB must be $I_n - I_{n-1}$. For the section BC of the nth monomer,

$$v_n - v_{n+1} = L\frac{dI_n}{dt} + I_nR_1, \tag{22}$$

where v_n and v_{n+1} are the voltages across AE and CF, respectively (see Fig. 6). Similarly, if the voltage across the capacitor is $V_n + V_0$, where V_0 is the bias voltage of the capacitor, we have

$$v_n = R_2(I_{n-1} - I_n) + V_0 + V_n. \tag{23}$$

Furthermore, the current through the section BD must be the rate of change of charge, Q_n, so that

$$I_{n-1} - I_n = \frac{dQ_n}{dt}. \tag{24}$$

From Eq. 22 we have

$$L\frac{dI_{n-1}}{dt} = v_{n-1} - v_n - I_{n-1}R_1 \tag{25}$$

and

$$L\frac{dI_n}{dt} = v_n - v_{n+1} - I_nR_1. \tag{26}$$

From Eq. 24,

$$L\frac{d^2Q_n}{dt^2} = L\frac{dI_{n-1}}{dt} - L\frac{dI_n}{dt}, \tag{27}$$

so from Eqs. 25, 26, and 27 we have

$$\begin{aligned} L\frac{d^2Q_n}{dt^2} &= v_{n-1} - v_n - I_{n-1}R_1 - (v_n - v_{n+1} - I_nR_1) \\ &= v_{n+1} + v_{n-1} - 2v_n + R_1(I_n - I_{n-1}). \end{aligned} \tag{28}$$

Using Eq. 23 in Eq. 28, we find

$$\begin{aligned} L\frac{d^2Q_n}{dt^2} &= LC_0(V_n - bV_n^2) \\ &= V_{n+1} + V_{n-1} - 2V_n - R_1C_0\frac{d}{dt}(V_n - bV_n^2) \\ &\quad - R_2C_0\left\{2\frac{d}{dt}(V_n - bV_n^2) - \frac{d}{dt}(V_{n+1} - bV_{n+1}^2)\right. \\ &\quad \left. - \frac{d}{dt}(V_{n-1} - bV_{n-1}^2)\right\}. \end{aligned} \tag{29}$$

A continuum approximation is now made by writing $V_n = V$ and using a Taylor expansion in a small spatial parameter a to give

$$\begin{aligned} V_{n+1} &= V + a(\partial_x V) + \frac{a^2}{2!}(\partial_{xx}V) + \frac{a^3}{3!}(\partial_{xxx}V) \\ &\quad + \frac{a^4}{4!}(\partial_{xxxx}V) + \cdots \end{aligned} \tag{30}$$

and

$$\begin{aligned} V_{n-1} &= V - a(\partial_x V) + \frac{a^2}{2!}(\partial_{xx}V) - \frac{a^3}{3!}(\partial_{xxx}V) \\ &\quad + \frac{a^4}{4!}(\partial_{xxxx}V) - \cdots, \end{aligned} \tag{31}$$

where, at this stage, we retain all derivatives up to the fourth order. From Eqs. 30 and 31 we find that

$$V_{n+1} - 2V_n + V_{n-1} = a^2(\partial_{xx}V) + \frac{2a^4}{4!}(\partial_{xxxx}V). \tag{32}$$

Using Eqs. 32, 30, and 31, Eq. 30 becomes

$$LC_0\frac{\partial^2}{\partial t^2}(V-bV^2)=a^2(\partial_{xx}V)+\frac{2a^4}{4!}(\partial_{xxxx}V)-R_1C_0\frac{\partial}{\partial t}(V-bV^2)+R_2C_0\frac{\partial}{\partial t}\left(a^2(\partial_{xx}V)+\frac{2a^4}{4!}(\partial_{xxxx}V)\right)$$
$$-R_2C_0b\frac{\partial}{\partial t}\left(2a^2\partial_{xx}V+2a^2(\partial_xV)^2+\frac{a^4}{6}V(\partial_{xxxx}V)+\frac{2a^4}{3}(\partial_xV)(\partial_{xxx}V)+\frac{a^4}{2}(\partial_{xx}V)^2\right). \quad (33)$$

We consider variations in time to be small compared to the constant background voltage and the nonlinear term in the capacitance to be of second order. Postulating that typical time derivatives are of order ε (where ε is some small parameter), the nonlinear voltage terms in the capacitance of order ε^2 and a of order ε, we retain only terms up to ε^3 in Eq. 33 to finally obtain:

$$LC_0\frac{\partial^2V}{\partial t^2}=a^2(\partial_{xx}V)+R_2C_0\frac{\partial}{\partial t}(a^2(\partial_{xx}V))$$
$$-R_1C_0\frac{\partial V}{\partial t}+R_1C_02bV\frac{\partial V}{\partial t}, \quad (34)$$

which will form the basis of our physical analysis of the ion conduction problem.

ANALYSIS OF THE VOLTAGE EQUATION

As a result of applying an input voltage pulse with an amplitude of ~200 mV and a duration of 800 μs to an actin filament, electrical signals were measured at the opposite end of the actin filament (Lader et al., 2000). This experiment indicates that actin filaments can support ionic waves in the form of axial nonlinear currents. The current measured in the process reached a peak value of ~13 nA and it lasted for ~500 μs. In a related earlier experiment (Lin and Cantiello, 1993), the wave patterns observed in electrically stimulated single actin filaments were remarkably similar to recorded solitary wave forms from various experimental studies on electrically stimulated nonlinear transmission lines (Kolosick et al., 1974; Lonngren, 1978; Noguchi, 1974). Considering the actin filament's highly nonlinear complex physical structure (Pollard and Cooper, 1986) and thermal fluctuations of the counterionic cloud from the average distribution (Oosawa, 1970, 1971), the observation of soliton-like ionic waves is consistent with the idea of actin filaments functioning as biological transmission lines.

Indeed, the soliton conformation theory for proteins involves charge displacement for ''resonant'' states within a particular structure as predicted by Davydov (see Davydov, 1982). However, in the case of actin in solution, the soliton behavior envisaged in our model is constrained to the ion clouds and represents the ''convective movement of ions'' along a one-dimensional polymer.

Based on the argument put forward above, in this section we analyze the solutions of Eq. 34 by looking for traveling waves. Thus the voltage becomes a function of an independent variable, the moving coordinate, $\zeta = x - v_0t$, so that $V = V(\zeta)$ and the equation becomes an ordinary differential equation, albeit nonlinear, where v_0 is the propagation velocity. Equation 34 then becomes

$$\frac{R_2a^2v_0}{L}\frac{d^3V}{d\zeta^3}+(v_0^2-c_0^2a^2)\frac{d^2V}{d\zeta^2}$$
$$+\left(\frac{2bR_1v_0}{L}V-\frac{R_1v_0}{L}\right)\frac{dV}{d\zeta}=0. \quad (35)$$

Here the parameter c_0^2 is defined by

$$c_0^2=\frac{1}{LC_0}. \quad (36)$$

Equation 35 may be integrated once to yield

$$\frac{R_2a^2v_0}{L}\frac{d^2V}{d\zeta^2}+(v_0^2-c_0^2a^2)\frac{dV}{d\zeta}$$
$$+\frac{1}{2}\left(\frac{2bR_1v_0}{L}V-\frac{R_1v_0}{L}\right)^2\frac{L}{2bR_1v_0}=d_0, \quad (37)$$

where d_0 is an integration constant.

We now outline two possible ways of proceeding with Eq. 37. In the first, we investigate the situation where voltage waves propagate at a maximum velocity, $v_0 = c_0a$, which leads to an elliptic form of equation. The second case involves a spectrum of excitations below the maximum velocity. This is obtained by mapping the problem onto the Fisher-Kolmogoroff equation.

Jacobi elliptic excitations

We first choose the propagation velocity, v_0, so that

$$v_0^2=c_0^2a^2=v_{max}^2. \quad (38)$$

For convenience we define a shifted voltage by

$$W=V-\frac{1}{2b}. \quad (39)$$

Equation 37 now becomes

$$\frac{d^2W}{d\zeta^2}=\frac{d_0L}{R_2a^2v_0}-\frac{b}{a^2}\frac{R_1}{R_2}W^2, \quad (40)$$

which is in standard elliptic form (Byrd and Friedman, 1971). This can be easily solved by multiplying both sides of Eq. 40 by $dW/d\zeta$ and then by $d\zeta$ and integrating both sides to obtain

$$\frac{1}{2}\left(\frac{dW}{d\zeta}\right)^2 = \frac{d_0 L}{R_2 a^2 v_0} W - \frac{b}{a}, \tag{41}$$

where f is yet another integration constant. Hence

$$\zeta - \zeta_0 = \int \frac{dW}{\sqrt{\left(\frac{2bR_1}{3a^2R_2}\right)\left(\frac{3d_0L}{bR_1v_0}W - W^3 + \frac{3a^2R_2f}{bR_1}\right)}}. \tag{42}$$

We define w_1, w_2, and w_3 to be the roots of the polynomial $P(W)$, which occurs in the denominator of Eq. 42, i.e.,

$$\begin{aligned} P(W) &= \left(\frac{2bR_1}{3a^2R_2}\right)\left(\frac{3d_0L}{bR_1v_0}W - W^3 + \frac{3a^2R_2f}{bR_1}\right) \\ &= \left(\frac{2bR_1}{3a^2R_2}\right)(W - w_1)(W - w_2)(w_3 - W) \end{aligned} \tag{43}$$

such that $w_1 < w_2 < w_3$ (see Fig. 7 for illustration). We then obtain

$$\sqrt{\frac{3a^2R_2}{2bR_1}}(\zeta - \zeta_0) = \int \frac{dW}{\sqrt{(W - w_1)(W - w_2)(w_3 - W)}}. \tag{44}$$

Using standard elliptic integral techniques (Byrd and Friedman, 1971), we note that

$$\int_y^{t_1} \frac{dt}{\sqrt{(t_1 - t)(t - t_2)(t - t_3)}} = g\,\mathrm{sn}^{-1}(\sin\phi, k), \tag{45}$$

where $g = (2/\sqrt{t_1 - t_3})$, $k = \sqrt{(t_1 - t_2)/(t_1 - t_3)}$ and $\sin\phi = \sqrt{(t_1 - y)/(t_1 - t_2)}$ with $t_1 > y \geq t_2 > t_3$, and by identifying

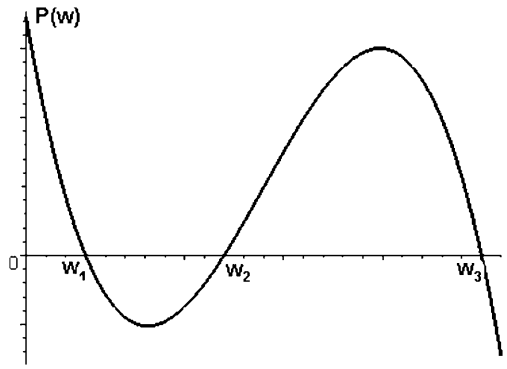

FIGURE 7 Plot of the cubic polynomial described in the right-hand side of Eq. 43.

$$\begin{aligned} t_1 &\to w_3 \\ t_2 &\to w_2 \\ t_3 &\to w_1 \end{aligned} \tag{46}$$

we obtain

$$\sqrt{\frac{3a^2R_2}{2bR_1}}(\zeta - \zeta_0) = \frac{2}{\sqrt{w_3 - w_1}}\,\mathrm{sn}^{-1}\left(\sqrt{\frac{w_3 - W}{w_3 - w_2}}, k\right). \tag{47}$$

Finally, we obtain an analytical solution in the form

$$W = w_3 - (w_3 - w_2)\mathrm{sn}^2\left(\frac{\sqrt{3a^2R_2(w_3 - w_1)}}{2\sqrt{2bR_1}}(\zeta - \zeta_0), k\right), \tag{48}$$

where $0 \leq k \leq 1$ with $k = \sqrt{(w_3 - w_2)/(w_3 - w_1)}$, where k is the elliptic modulus. The solution in Eq. 48 is illustrated in Fig. 8 *a* for $k = 0.8$ as an example. Note that Eq. 48 describes an infinite parametric family of elliptic waves classified by the elliptic modulus k. When $k \to 0$, the sn(·) function tends to the trigonometric sine function, and that corresponds to the roots w_2 and w_3 coalescing. Simultaneously, the amplitude of the wave vanishes and so does the wavelength. On the other hand, when the roots w_2 and w_1 coalesce, the elliptic modulus $k \to 1$ and we can integrate Eq. 44 easily, which we carry out below.

Thus we define the elementary integral, which is evaluated as

$$\begin{aligned} \zeta - \zeta_0 &= \int \frac{dW}{(W - w_1)\sqrt{w_2 - W}} \\ &= -\frac{1}{\sqrt{w_2 - w_1}}\cosh^{-1}\left(2\frac{(w_2 - w_1)}{W - w_1} - 1\right). \end{aligned} \tag{49}$$

Finally, we obtain

$$W = w_1 + \frac{2(w_2 - w_1)}{1 + \cosh\left(\sqrt{w_2 - w_1}(\zeta - \zeta_0)\right)}. \tag{50}$$

This solution is illustrated in Fig. 8 *b*, and it represents a localized bump propagating with the velocity, v_0. Both the family of propagating waves in Eq. 48 and the solitary wave in Eq. 50 travel at the velocity v_0, which can be estimated using the parameters obtained in the previous section, and we find

$$v_{\max} = 3 \times 10^5 \mathrm{m.s}^{-1}. \tag{51}$$

This number is astonishingly high, and it indicates that the nature of the wave is purely electromagnetic involving a resonant energy transfer from one *LC* element to the neighbor with no apparent loss as can be seen from Eq. 37,

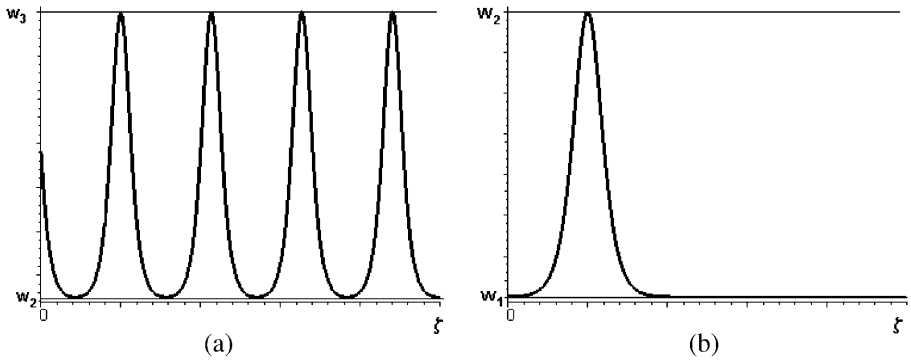

FIGURE 8 (*a*) Plot of the solution W represented by Eq. 48 for the parameter $k = 0.8$. (*b*) Plot of the solution W represented by Eq. 50.

where the dissipative first derivative disappears. Furthermore, resistivity of the solution does not affect the propagation velocity since the ions themselves are not transported from one element to the next but simply get excited and de-excited. Although this form of resonant energy transfer is not impossible, it would require a very special mechanism for excitation, and we leave this tantalizing speculation up to future experimental studies. Hence we turn to the second method of solving Eq. 37 in the hope of finding a more realistic solution that would correspond to the already observed effects.

Fisher-Kolmogoroff propagation modes

Fisher (1937) proposed a one-dimensional version of the Fisher-Kolmogoroff equation to describe the spread of an advantageous gene in a population. It takes the form

$$\frac{\partial M}{\partial t} = rM\left(1 - \frac{M}{\kappa}\right) + D\frac{\partial^2 M}{\partial x^2}. \tag{52}$$

In this equation, M denotes a population density and the factor $h = rM(1 - (M/\kappa))$ is the logistic population growth, where r is the linear reproduction rate and κ the carrying capacity of the environment. D is a diffusion constant. We consider traveling waves in an independent variable $\zeta = x - \overline{v}t$, where $\overline{v}$ is an arbitrary propagation velocity, in which case Eq. 52 becomes

$$D\frac{d^2M}{d\zeta^2} + \overline{v}\frac{dM}{d\zeta} - \frac{r}{\kappa}M^2 + rM = 0. \tag{53}$$

The Fisher equation, of course, and particularly its traveling wave solutions, have been widely studied including more generalized nonlinear terms (Kolmogoroff et al., 1937) and there is an extensive bibliography where full discussions may be found (Britton, 1986; Fife and McLeod, 1977). To show the existence of traveling waves in a simple way, we note that if we change the dependent variable, M, to U, where $U = M/\kappa$ and the independent variable ζ to $\eta = \sqrt{r/D}\zeta$, Eq. 53 becomes

$$\frac{d^2U}{d\eta^2} + c\frac{dU}{d\eta} + U(1 - U) = 0, \tag{54}$$

where $c = \overline{v}/\sqrt{Dr}$. It is then a trivial matter to show that

$$U = \frac{1}{(1 + pe^{q\eta})^s} \tag{55}$$

is a traveling wave solution of Eq. 54, where we find $s = 2$, $q^2 = 1/6$, and the parameter p remains arbitrary. The kink of Eq. 55 propagates from left to right with $c = 5/\sqrt{6} \simeq 2.041$ (see, for example, Fig. 9 *a*).

Equation 54 also admits a one-parameter family of nontrivial standing wave solutions (structures stationary in time). The explicit expressions of these stationary solutions

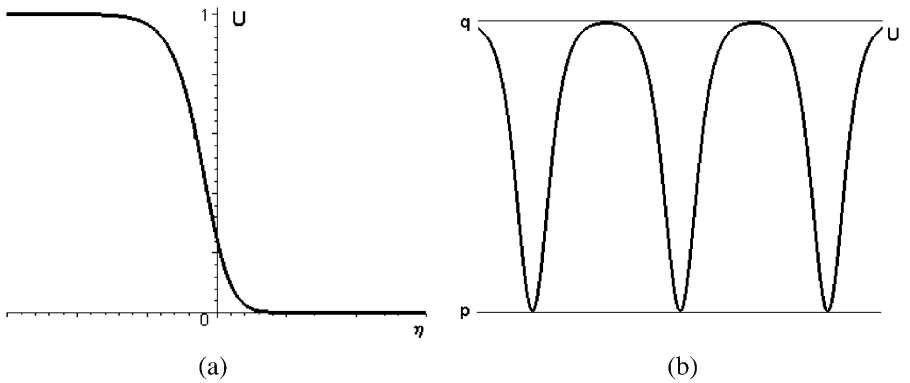

FIGURE 9 (*a*) Plot of the solution of Eq. 54 defined by Eq. 55. (*b*) Plot of the solution of Eq. 54 defined by Eq. 56.

can be obtained in terms of the Jacobian elliptic functions (see for illustration Fig. 9 *b*)

$$U(x) = p + (q-p)\mathrm{sn}^2\left(\frac{1}{g}\sqrt{\frac{2}{3}}x, k\right), \tag{56}$$

where p and q are maximum and minimum amplitudes of U, respectively, and $g = (2/\sqrt{1.5-q-2p})$ (Brazhnik and Tyson, 1999).

We show, in this section, that the voltage equation, Eq. 37, may be cast into the Fisher form. To this end, denoting $dV/d\zeta$ by V', we write the voltage equation Eq. 37 as

$$V'' + \lambda V' + \gamma V^2 + \delta V + \varepsilon = 0, \tag{57}$$

where

$$\lambda = \frac{(v_0^2 - c_0^2 a^2)L}{R_2 a^2 v_0}, \qquad \gamma = \frac{bR_1}{a^2 R_2}$$
$$\delta = \frac{-R_1}{R_2 a^2}, \qquad \varepsilon = \frac{R_1}{R_2}\frac{1}{4ba^2} - \frac{d_0 L}{R_2 a^2 v_0}.$$

To compare the voltage equation with Eq. 53, we must first linearly transform Eq. 57 to ensure that various parameters which appear have the correct sign. We define the corresponding change of variable as

$$V = \alpha W + \beta, \tag{58}$$

where α and β are constants to be determined. Thus, Eq. 57 is now expressed as follows:

$$W'' + \lambda W' + \gamma\alpha W^2 + (2\gamma\beta + \delta)W + \frac{\gamma\beta^2}{\alpha} + \frac{\delta\beta}{\alpha} + \frac{\varepsilon}{\alpha} = 0. \tag{59}$$

By identifying the coefficients of Eq. 59 with the coefficients of Eq. 53. we postulate $W = M$ and determine the constants α and β to be

$$\alpha = \frac{-\sqrt{\delta^2 - 4\gamma\varepsilon}}{\gamma\kappa} \quad \text{and} \quad \beta = \frac{-\delta + \sqrt{\delta^2 - 4\gamma\varepsilon}}{2\gamma}. \tag{60}$$

Thus the new dependent voltage, W, which is a scaled and shifted form of the original voltage, V, satisfies a one-dimensional Fisher equation like that in Eq. 53. Hence the traveling wave solution described in Eq. 55 can be used to define the solution V of Eq. 57 as

$$V = \frac{1}{2b} + \sqrt{\frac{d_0 L}{bR_1 v_0}} \times \left(1 - \frac{2}{\left(1 + pe^{q\sqrt{(2/a^2R_2)\sqrt{(bd_0R_1L/v_0)}\zeta}}\right)^s}\right). \tag{61}$$

It is worth pointing out that all the physical parameters appear in the mathematical description of the kink. The capacitance dependence arises from $\overline{v}$ or $v_{\max}$. R_1, R_2, and L determine the shape of the kink such that the amplitude is proportional to $\sqrt{L}$ and inversely proportional to $\sqrt{R_1}$ and $\sqrt{b}$. Note that in the limit of the nonlinearity coefficient b tending to zero, the solution becomes singular and hence unphysical. The width of the kink is proportional to $\sqrt{R_2}$ and the lattice constant a and inversely proportional to the quartic root of bR_1L. We point out that there is a dependence of these physical parameters on the chemical state of the solution and the temperature under which experiments are carried out. The values of the resistance depend on the temperature, the viscosity, and concentration of the solution. In Fig. 10, we show the only available experimental data supporting the presence of soliton waves along actin filament. However, in

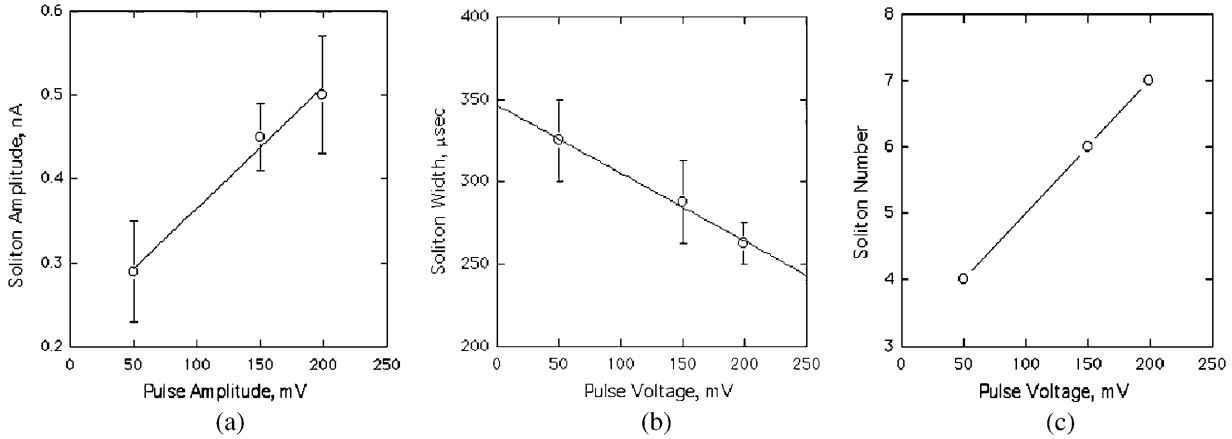

FIGURE 10 Experimental plots of (*a*) the soliton amplitude versus the pulse amplitude, (*b*) the soliton width versus the pulse voltage, and (*c*) the number of solitons generated versus the pulse voltage, following Lin and Cantiello (1993).

view of the presence of only three data points, a quantitative comparison between our predictions and experiment is not warranted at present.

Note that the actual propagation velocity for the traveling kink solution is given by

$$\overline{v} = \frac{D\left(v_0^2 - v_{\max}^2\right)L}{R_2 a^2 v_0}. \tag{62}$$

We have established earlier that $v_{\max} = 3 \times 10^5\,\mathrm{m.s}^{-1}$ and the values of the remaining constants have also been determined except for the diffusion constant, D. However, it is well known that the diffusion constant for ions in aqueous solutions is on the order of $10^{-9}\,\mathrm{m}^2.\mathrm{s}^{-1}$ (Tuszynski and Dixon, 2001). The velocity parameter, v_0, determines the unidirectional flow of the ions, whereas $\overline{v}$ is the velocity of the moving nonlinear wave. With the above estimates we find that

$$\overline{v} \simeq \frac{10^8\left(\mathrm{m.s}^{-1}\right)^2}{v_0}. \tag{63}$$

Interestingly, this indicates that slow linear waves give rise to fast nonlinear propagation of localized ionic clusters. We expect that v_0 is much less than $v_{\max}$. With this in mind, and the knowledge that the velocity of ion flows in physiological situations, such as action-potential propagation (Alberts et al., 1998), ranges between 0.1 and 10 $\mathrm{m.s}^{-1}$, we estimate the corresponding nonlinear wave velocities, $\overline{v}$, to be such that

$$100\,\mathrm{m.s}^{-1} \geq \overline{v} \geq 1\,\mathrm{m.s}^{-1}. \tag{64}$$

This study only provides an indication as to a realistic model of actin that can support soliton-like ionic traveling waves. Modeling relies on data constrained by experimental conditions, and/or assumptions made, including the charge density, which is calculated based on the net surface charges of actin. It should also be considered that soliton velocity is directly proportional to the magnitude of the stimulus, which in a biological setting has not been formally described. Actin interacts with a number of ion channels, of different ionic permeability, and conductance. Thus, it is expected that channel opening, single-channel currents, and other channel properties, including the resting potential of the cell, may significantly modify the amplitude and velocity of the soliton-supported waves. This should correlate with the velocity of the traveling waves along channel-coupled filaments. Other parameters that may play a role in this type of electrodynamic interaction are the local ionic gradients and the regulatory role of actin-binding proteins, which can help ''focus'' the conductive medium or otherwise impair wave velocity.

CONCLUSIONS

Motivated by several intriguing experiments (Cantiello et al., 1991; Lin and Cantiello, 1993) that indicated the possibility of ionic wave generation along actin filaments, we have developed a physical model that provides a framework for the analysis of these waves. The background for the model is the molecular structure of an actin filament and its interaction with solvent ions. Following earlier ideas, we have represented the filament with the surrounding ions as an electrical transmission line with L, R, and C elements in it. One of the key aspects is the nonlinearity of the associated capacitance (Ma et al., 1999; Wang et al., 1999) that eventually gives rise to the self-focusing of the ionic waves. The equations developed for the model originate from the application of Kirchhoff's laws to the *LRC* resonant circuit of a model actin monomer in a filament. We then took the continuum limit and determined second order partial differential equations for the spatio-temporal dependence of voltage. These nonlinear equations were eventually solved using two different approaches. The first ansatz resulted in a zero dissipation state (due to the absence of resistive terms) corresponding to an absolute maximum velocity of propagation. This, however, implies a purely electromagnetic disturbance propagating resonantly from node to node in the circuit. A more physically realistic case involved mapping our equation onto the Fisher-Kolmogoroff equation with the attendant elliptic and topological solitonic solutions. The elliptic waves were stationary in time and may lead to the establishment of spatial periodic patterns of ionic concentration. Perhaps the most important finding obtained in this work is the existence of the traveling wave kink, which describes a moving transition region between a high and low ionic concentration due to the corresponding intermonomeric voltage gradient. The velocity of propagation was estimated to range between 1 and 100 $\mathrm{m.s}^{-1}$, depending on the characteristic properties of the electrical circuit model. It is noteworthy that these values overlap with action potential velocities in excitable tissues (Hille, 1992).

We believe that these findings may have important consequences for our understanding of the signaling and ionic transport at intracellular level. Extensive new information (Janmey, 1998) indicates that actin filaments are both directly (Chasan et al., 2002) and indirectly linked to ion channels in both excitable and nonexcitable tissues, providing a potentially relevant electrical coupling between these current generators (i.e., channels), and intracellular transmission lines (i.e., actin filaments). Furthermore, actin filaments are crucially involved in cell motility and, in this context, they are known to be able to rearrange their spatial configuration. It is tantalizing to speculate that ionic waves surrounding these filaments may participate or even trigger the rearrangement of intracellular actin networks. In nerve cells, actin filaments are mainly located in the synaptic bouton region. Again, it would make sense for electrical signals supported by actin filaments to help trigger neurotransmitter release through voltage-modulated membrane deformation leading to exocytosis (Segel and Parnas, 1991). Actin is also prominent in postsynaptic dendritic

spines, and its dynamics within dendritic spines has been implicated in the postsynaptic response to synaptic transmission. Kaech et al. (1999) have shown that general anesthetics inhibit this actin-mediated response. Incidentally, it is noteworthy that Claude Bernard showed also that the anesthetic gas chloroform inhibited cytoplasmic movement in slime mold. Actin structural dynamics plays a significant role in synaptic plasticity and neuronal function. Among functional roles of actin in neurons, we mention in passing glutamate receptor channels that are implicated in long-term potentiation. It is therefore reasonable to expect ionic wave propagation along actin filaments to lead to a broad range of physiological effects.

J. M. Dixon thanks the staff and members of the Physics Department of the University of Alberta for all their kindness and thoughtfulness during his stay.

This project has been supported by grants from the Natural Sciences and Engineering Research Council and Mathematics of Information Technology and Complex Systems. S. Portet acknowledges support from the Bhatia Post-Doctoral Fellowship Fund.

REFERENCES

Alberts, B., D. Bray, A. Johnson, J. Lewis, M. Raff, K. Roberts, and P. Walter. 1998. Essential Cell Biology: An Introduction to the Molecular Biology of the Cell. Garland Science Publishing, New York.

Anderson, C., and M. Record. 1990. Ion distributions around DNA and other cylindrical polyions: theoretical descriptions and physical implications. *Annu. Rev. Biophys. Biophys. Chem.* 19:423–465.

Baverstock, K., and R. Cundall. 1988. Solitons and energy transfer in DNA. *Nature.* 332:312–313.

Brazhnik, P., and J. Tyson. 1999. On traveling wave solutions of Fisher's equation in two spatial dimensions. *SIAM J. Appl. Math.* 60:371–391.

Britton, N. 1986. Reaction-Diffusion Equations and Their Applications to Biology. Academic Press, New York.

Byrd, P., and M. Friedman. 1971. Handbook of Elliptic Integrals for Engineers and Scientists. Springer, Berlin.

Cantiello, H., C. Patenande, and K. Zaner. 1991. Osmotically induced electrical signals from actin filaments. *Biophys. J.* 59:1284–1289.

Chasan, B., N. Geisse, K. Pedatella, D. Wooster, M. Teintze, M. Carattino, W. Goldmann, and H. Canteillo. 2002. Evidence for direct interaction between actin and the cystic fibrosis transmembrane conductance regulator. *Eur. Biophys. J.* 30:617–624.

Coppin, C., and P. Leavis. 1992. Quantitation of liquid-crystalline ordering in F-actin solution. *Biophys. J.* 63:794–807.

Davydov, A. S. 1982. Biology and Quantum Mechanics. Pergamon Press, Oxford, UK.

Fife, P., and J. McLeod. 1977. The approach of solutions of nonlinear diffusion equations to traveling wave solutions. *Arch. Rat. Mech. Anal.* 65:335–361.

Fisher, R. 1937. The wave of advance of advantageous genes. *Ann. Eugenics.* 7:353–369.

Fröhlich, H. 1975. The extraordinary dielectric properties of biological materials and the action of enzymes. *Proc. Natl. Acad. Sci. USA.* 72:4211–4215.

Fröhlich, H. 1984. Nonlinear Electrodynamics in Biological Systems. Plenum Press, New York.

Furukawa, R., R. Kundra, and M. Fechkeimer. 1993. Formation of liquid crystals from actin filaments. *Biochemistry.* 32:12346–12352.

Hagan, S., S. R. Hameroff, and J. A. Tuszynski. 2002. Quantum computation in brain microtubules: decoherence and biological feasibility. *Phys. Rev. E.* 65:1–10.

Hameroff, S., A. Nip, M. Porter, and J. A. Tuszynski. 2002. Conduction pathways in microtubules, biological quantum computation, and consciousness. *Biosystems.* 64:149–168.

Hille, B. 1992. Ionic Channels of Excitable Membranes. Sinauer Associates, Sunderland, MA.

Holmes, K., D. Popp, W. Gebhard, and W. Kabsch. 1990. Atomic model of the actin filament. *Nature.* 347:44–49.

Janmey, P. 1998. The cytoskeleton and the cell signaling: component localization and mechanical coupling. *Physiol. Rev.* 78:763–781.

Kabsch, W., H. Mannberg, D. Suck, E. Pai, and K. Holmes. 1990. Atomic structure of the actin: DNAse I complex. *Nature.* 347:37–44.

Kaech, S., H. Brinkhaus, and A. Matus. 1999. Volatile anesthetics block actin-based motility in dendritic spines. *Proc. Natl. Acad. Sci. USA.* 96: 10433–10437.

Kobayasi, S. 1964. Effect of electric field on F-actin orientated by flow. *Biochim. Biophys. Acta.* 88:541–552.

Kobayasi, S., H. Asai, and F. Oosawa. 1964. Electric birefringence of actin. *Biochim. Biophys. Acta.* 88:528–540.

Kolmogoroff, A., I. Petrovsky, and N. Piscounoff. 1937. Study of the diffusion equation with growth of the quantity of matter and its application to a biological problem. *Moscow Univ. Bull. Math.* 1:1–25.

Kolosick, J., D. Landt, H. Hsuan, and K. Lonngren. 1974. Properties of solitary waves as observed on a non-linear dispersive transmission line. *Proc. IEEE.* 62:578–581.

Lader, A., H. Woodward, E. Lin, and H. Cantiello. 2000. Modeling of ionic waves along actin filaments by discrete electrical transmission lines. *METMBS '00 International Conference.* 77–82.

Le Bret, M., and B. H. Zimm. 1984. Distribution of counterions around a cylindrical polyelectrolyte and Manning's condensation theory. *Biopolymers.* 23:287–312.

Lin, E., and H. Cantiello. 1993. A novel method to study the electrodynamic behavior of actin filaments. Evidence of cable-like properties of actin. *Biophys. J.* 65:1371–1378.

Lonngren, K. 1978. Observations of solitons on non-linear dispersive transmission lines. *In* Solitons in Action. K. E. Lonngren and A. C. Scott editors. Academic Press, New York. 127–152.

Ma, Z., J. Wang, and H. Guo. 1999. Weakly nonlinear ac response: theory and application. *Phys. Rev. B.* 59:7575–7578.

MacInnes, D. A. 1961. The Principles of Electrochemistry. Dover Publications, London.

Manning, G. 1969. Limiting laws and counterion condensation in polyelectrolyte solutions I. Colligative properties. *J. Chem. Phys.* 51:924–933.

Manning, G. S. 1978. The molecular theory of polyelectrolyte solutions with applications to the electrostatic properties of polynucleotides. *Q. Rev. Biophys.* 2:179–246.

Mavromatos, N. E. 1999. Quantum-mechanical coherence in cell microtubules: a realistic possibility? *Bioelectrochem. Bioenerg.* 48:273–284.

Noguchi, A. 1974. Solitons in a non-linear transmission line. *Electronics and Communications in Japan.* 57:9–13.

Oosawa, F. 1970. Counterion fluctuation and dielectric dispersion in linear polyelectrolytes. *Biopolymers.* 9:677–688.

Oosawa, F. 1971. Polyelectrolytes. Marcel Dekker, New York.

Ostrovskii, L. 1977. Shock waves and solitons (selected problems). *Radiophysics and Quantum Electronics.* 18:464–486.

Parodi, M., B. Bianco, and A. Chiabrera. 1985. Toward molecular electronics. Self-screening of molecular wires. *Cell Biophys.* 7:215–235.

Pollard, T., and J. Cooper. 1986. Actin and actin-binding proteins. a critical evaluation of mechanisms and functions. *Annu. Rev. Biochem.* 55:987–1035.

Rullman, J., and P. van Duijnem. 1990. Potential energy models of biological macromolecules: a case ab initio quantum chemistry. *Rep. Mol. Theory.* 1:1–21.

Sataric, M., J. Tuszynski, and R. Zakula. 1993. Kink-like excitations as an energy-transfer mechanism in microtubules. *Phys. Rev. E.* 48:589–597.

Segel, L., and H. Parnas. 1991. What controls the exocytosis of neurotransmitters. *In* Biologically Inspired Physics. L. Peliti, editor. Plenum Press, New York.

Sept, D., J. Xu, T. Pollard, and J. McCammon. 1999. Annealing accounts for the length of actin filaments formed by spontaneous polymerization. *Biophys. J.* 77:2911–2919.

Tang, J., and P. Janmey. 1996. The polyelectrolyte nature of F-actin and the mechanism of actin bundle formation. *J. Biol. Chem.* 271:8556–8563.

Torbet, J., and M. Dickens. 1984. Orientation of muscle actin in strong magnetic fields. *FEBS Lett.* 173:403–406.

Tuszyński, J. A., and J. M. Dixon. 2001. Biomedical Applications of Introductory Physics. John Wiley and Sons, New York.

Wang, B. G., X. A. Zhao, J. Wang, and H. Guo. 1999. Nonlinear quantum capacitance. *Appl. Phys. Lett.* 74:2887–2889.

Zimm, B. 1986. Use of the Poisson-Boltzmann equation to predict ion condensation around polyelectrolytes. *In* Coulombic Interactions in Macromolecular Systems. A. Gisenhart and F. E. Bailey, editors. American Chemical Society, Washington, DC. 212–215.